Anti-cluster Decay and Anti-alpha Decay of Antimatter nuclei

D. N. Poenaru,[1,2,*] R. A. Gherghescu,[1] and W. Greiner[2]

[1] *Horia Hulubei National Institute of Physics and Nuclear Engineering (IFIN-HH), P.O. Box MG-6, RO-077125 Bucharest-Magurele, Romania*

[2] *Frankfurt Institute for Advanced Studies (FIAS), Ruth-Moufang-Str. 1, 60438 Frankfurt am Main, Germany*

(Dated:)

Abstract

A broad extension of periodic system into the sector of antimatter could be possible sometimes in a remote future. We expect that anti-alpha spontaneous emission from an antimatter nucleus will have the same Q-value and half-life as alpha emission from the corresponding mirror nucleus. This is the consequence of the invariance of binding energy as well as of the surface and Coulomb energy when passing from matter to antimatter nuclei with the the same mass number and the same atomic number. The Q-values and half-lives of all measured up to now 27 cluster radioactivities are given together with Q-values and half-lives of the most important competitor — α decay. The lightest anti-alpha emitter, $^{8}\bar{B}e$, will have a very short half-life of about $81.9 \cdot 10^{-18}$ s.

PACS numbers: 36.10.-k, 23.70.+j, 23.60.+e, 21.10.Tg

* poenaru@fias.uni-frankfurt.de

I. INTRODUCTION

In 1928 Dirac predicted the existence of negative energy states of electrons [1] when he developed his famous relativistic wave equation for massive fermions. The antimatter character of these states became clear in 1933 after discovery of the positron (the antielectron) in cosmic radiation by Anderson [2].

Individual anti-particles are produced by particle accelerators and in some types of radioactive decay. Antiprotons ($\bar{p}$) [3] were observed in 1955 by Segrè and Chamberlain. The antineutron was discovered in proton-proton collisions at the Bevatron (Lawrence Berkeley National Laboratory) by Cork et al. in 1956 [4]. Antiprotons are produced at Fermilab for collider physics operations in the Tevatron. Other accelerators with complex projects for antimatter physics are the Relativistic Heavy Ion Collider (RHIC) at Brookhaven National Laboratory, LHC at CERN, and in the future Facility for Antiproton and Ion Research (FAIR)'s high-energy storage ring in Darmstadt [5].

Until now it was established in all experiments that every antiparticle has the same mass with its particle counterpart; they differ essentially by the sign of electric charge. Also every antinucleus has the same mass or binding energy as its mirror nucleus [6].

Anti-atoms are difficult to produce; the simplest one — the antihydrogen ($\bar{H}$) was produced, cooled and confined [7] for about 1000 s [8–11]. At the beginning the Low Energy Antiproton Ring (LEAR) at CERN was used. This device decelerated the antiprotons and stored them in a ring. The antimatter helium-4 nucleus, ${}^4\bar{H}e$, or anti-α, consists of two antiprotons and two antineutrons (baryon number $B = -4$) [12]. This is the heaviest observed antinucleus to date. It seems that the next one, antilithium, has an extremely low production rate.

It will be a long way to produce a rich diversity of more complex antinuclei justifying a broad extension of periodic system into the sector of antimatter and strangeness [13]. Nevertheless in this work we try to understand whether their decay modes by anti-α and anti-cluster spontaneous emission would differ from α decay and cluster radioactivity [14–16] of corresponding mirror nuclei.

II. POTENTIAL BARRIERS

Let us assume that a binary decay mode (e.g. anti-alpha decay, anti-cluster decay or spontaneous fission) of a parent anti-nucleus, ${}^{A}\bar{Z}$, leads to an emitted anti-cluster, ${}^{A_e}\bar{Z}_e$, and a daughter anti-nucleus, ${}^{A_d}\bar{Z}_d$:

$$ {}^{A}\bar{Z} \ \rightarrow \ {}^{A_d}\bar{Z}_d \ + \ {}^{A_e}\bar{Z}_e \tag{1}$$

with conservation of baryon numbers. Alternatively the subscript d may be denoted with 1 and e with 2. By definition, the number of antiprotons of an antinucleus is equal with the number of protons of the corresponding nucleus. The same is true for the number of antineutrons and of neutrons. Consequently, there is a good reason to assume that every anti-cluster, ${}^{A_e}\bar{Z}_e$, will have the same binding energy as the cluster ${}^{A_e}Z_e$, and similarly the binding energy of the daughter anti-nucleus, ${}^{A_d}\bar{Z}_d$, will be identical with that of the daughter, ${}^{A_d}Z_d$, and the binding energy of the parent anti-nucleus, ${}^{A}\bar{Z}$, is identical with that of the parent ${}^{A}Z$. The released energy

$$Q = [M - (M_d + M_e)]c^2 \tag{2}$$

can be calculated using the last evaluation of experimental data for atomic masses [17]. In this eq. c is the light velocity, M, M_d, M_e are the masses of parent, daughter and emitted nucleus.

In general the ratio of $Z/A \neq Z_d/A_d \neq Z_e/A_e$ meaning that the three partners have different charge densities. One can take into consideration the difference in charge densities [18] by assuming uniformity in each of the two fragments. In this way the nuclear volume $V = V_1 + V_2$ is divided in two parts, each of them being homogeneously charged with a density

$$\rho_e(\mathbf{r}) = \begin{cases} \rho_{1e}, \ \mathbf{r} \in V_1 \\ \rho_{2e}, \ \mathbf{r} \in V_2 \end{cases} \tag{3}$$

During the decay process from one parent to two fragments there is a potential barrier which determines the metastability of any anti-nucleus. It is penetrated by quantum mechanical tunnelling as was shown by Gamow in 1928 for alpha decay of nuclides [19].

For cylindrical symmetry the simplest parametrization of the shape during this process, with only one deformation parameter (the volume and the radius of the emitted fragment

are conserved), is that of two intersected spheres assumed in the two-center shell model [20]. The radius of the initial spherical anti-nucleus is $R_0 = r_0 A^{1/3}$ and the radii of the two fragments are $R_e = r_0 A_e^{1/3}$ and $R_d = r_0 A_d^{1/3}$. Within Myers-Swiatecki's liquid drop model (LDM) [21] the radius constant $r_0 = 1.2249$ fm and in the Yukawa-plus-Exponential model (Y+EM) [22] $r_0 = 1.16$ fm. During the overlapping stage the separation distance of the two fragments increases from an initial value $R_i = R_0 - R_e$ to the touching point value $R_t = R_e + R_d$. It is convenient to use the deformation parameter $\xi = (R - R_i)/(R_t - R_i)$ equal to unity at the touching point $R = R_t$.

We apply the macroscopic-microscopic method [23] to calculate the deformation energy, E_{def}, according to which a small shell and pairing correction δE is added to the macroscopic phenomenological model deformation energy obtained by summing the surface and Coulomb energy due to the strong and electrostatic forces:

$$E_{def} = (E_s - E_s^0) + (E_C - E_C^0) \tag{4}$$

where $E_s^0 = a_{20} A^{2/3} = a_s(1-\kappa_s I^2)A^{2/3}$ and $E_C^0 = 3e^2 Z^2/(5r_0 A^{1/3}$ correspond to the spherical parent with $a_s = 17.9439$ MeV, $I = (N - Z)/A$ and $\kappa_s = 1.7826$ within LDM.

The proton levels and neutron levels of a single particle shell model, e.g. two center shell model [24], allowing to calculate [23] the shell and pairing correction, δE, are different because protons are electrically charged. In the same way for antinuclei the antiproton levels should be different from antineutron levels but the antiproton levels would be identical with proton levels and antineutron levels identical with neutron levels.

A. Strong interaction

During the deformation from $R = R_i$ to $R = R_t$ the strong interaction is responsible for the surface energy. The strong force acts between antinucleons in the same manner it acts between nucleons; the electric charge doesn't play any role. For a number of antinucleons equal to that of nucleons it will have the same effect. The deformation dependent term is obtained by division with E_s^0:

$$B_s = \frac{E_s}{E_s^0} = \frac{a_{21}}{a_{20}} B_{s1} + \frac{a_{22}}{a_{20}} B_{s2} \tag{5}$$

with $a_{21} \neq a_{22} \neq a_{20}$ taking into account the difference in charge densities. B_{s1} and B_{s2} are proportional with surface areas of the fragments:

$$B_{s1} = \frac{d^2}{2} \int_{-1}^{x_c} \left[y^2 + \frac{1}{4} \left(\frac{dy^2}{dx} \right)^2 \right]^{1/2} dx \tag{6}$$

$$B_{s2} = \frac{d^2}{2} \int_{x_c}^{1} \left[y^2 + \frac{1}{4} \left(\frac{dy^2}{dx} \right)^2 \right]^{1/2} dx \tag{7}$$

where $d = (z'' - z')/2R_0$ is the length of the deformed antinucleus divided by the diameter of the spherical shape and x_c is the position of separation plane between fragments with -1, +1 intercepts on the symmetry axis (surface equation $y = y(x)$ or $y_1 = y(x')$).

B. Coulomb interaction

We can see that not only the surface energy but also the Coulomb energy is invariant when passing from matter to antimatter because in the following general relationship [25] the charge density appears as a product of $\rho_e(\mathbf{r})\rho_e(\mathbf{r_1})$:

$$E_c = \frac{1}{2} \int_{V_n} \int \frac{\rho_e(\mathbf{r})\rho_e(\mathbf{r}_1) d^3r d^3r_1}{|\mathbf{r} - \mathbf{r}_1|} \tag{8}$$

See also the expression of E_C^0 above.

For fragments with different charge densities by dividing with E_C^0 we obtain

$$B_c = \frac{E_c}{E_c^0} = \left(\frac{\rho_{1e}}{\rho_{0e}} \right)^2 B_{c1} + \frac{\rho_{1e}\rho_{2e}}{\rho_{0e}^2} B_{c12} + \left(\frac{\rho_{2e}}{\rho_{0e}} \right)^2 B_{c2} \tag{9}$$

explicitly showing the electrostatic self-energies and the interaction of two fragments. For binary systems with different charge densities and axially-symmetric shapes, we got

$$B_{c1} = b_c \int_{-1}^{x_c} dx \int_{-1}^{x_c} dx' F(x, x') \tag{10}$$

$$B_{c12} = b_c \int_{-1}^{x_c} dx \int_{x_c}^{1} dx' F(x, x') \tag{11}$$

$$B_{c2} = b_c \int_{x_c}^{1} dx \int_{x_c}^{1} dx' F(x, x') \tag{12}$$

where $b_c = 5d^5/8\pi$ and d, x_c were defined in the previous subsection. The integrand is given by

$$\begin{aligned} F(x, x') = \{ yy_1 \frac{K - 2D}{3} \left[2(y^2 + y_1^2) - (x - x')^2 + \frac{3}{2}(x - x') \left(\frac{dy_1^2}{dx'} - \frac{dy^2}{dx} \right) \right] \\ + K \left\{ \frac{y^2 y_1^2}{3} + \left[y^2 - \frac{x - x'}{2} \frac{dy^2}{dx} \right] \left[y_1^2 + \frac{x - x'}{2} \frac{dy_1^2}{dx'} \right] \right\} \} a_\rho^{-1} \end{aligned} \tag{13}$$

where $D = (K - K')/k^2$; K and K' are the complete elliptic integrals of the first and second kind, respectively:

$$K(k) = \int_0^{\pi/2} (1 - k^2 \sin^2 t)^{-1/2} dt \ ; \ K'(k) = \int_0^{\pi/2} (1 - k^2 \sin^2 t)^{1/2} dt \tag{14}$$

and $a_\rho^2 = (y+y_1)^2 + (x-x')^2$, $k^2 = 4yy_1/a_\rho^2$. The elliptic integrals are calculated by using the Chebyshev polynomial approximation. For $x = x'$ the function $F(x, x')$ is not determined. In this case, after removing the indetermination, we get $F(x, x') = 4y^3/3$.

C. Examples

In figures 1 and 2 (top panel) we present two examples of potential barriers calculated within LDM and Y+EM for spontaneous emission of $^{34}\bar{S}i$ from $^{242}C\bar{m}$ and $^{14}\bar{C}$ radioactivity of $^{250}C\bar{f}$, respectively. In both cases it is clear that within Y+EM the strong interaction continues to act, as a proximity force even for separated fragments, $R > R_t$, as long as the the tip separation distance remains small enough; the interaction energy is maximum at certain distance $R_m > R_t$. For spherical fragments there is an analytical relationships of interaction term:

$$E_{Y12} = -4 \left(\frac{a}{r_0}\right)^2 \sqrt{a_{21} a_{22}} \left[g_1 g_2 \left(4 + \frac{R}{a}\right) - g_2 f_1 - g_1 f_2 \right] \frac{\exp(-R/a)}{R/a} \tag{15}$$

$$g_k = \frac{R_k}{a} \cosh\left(\frac{R_k}{a}\right) - \sinh\left(\frac{R_k}{a}\right) \ ; \ f_k = \left(\frac{R_k}{a}\right)^2 \sinh\left(\frac{R_k}{a}\right) \tag{16}$$

where $a = 0.68$ fm is the diffusivity parameter and $a_2 = a_s(1 - \kappa I^2)$, $a_s = 21.18466$ MeV, $\kappa = 2.345$.

The contribution of surface, E_s, and Coulomb energy, E_C, to the LDM potential barrier is plotted at the bottom of figures 1 and 2. The potential barrier height is the result of adding an increasing with separation distance surface energy up to the touching point with a decreasing electrostatic energy up to infinity.

III. HALF-LIVES

The experimental data on halflives against cluster radioactivity [26, 27], T_c, and α decay, T_α, are given in Table I, together with Q-values, updated using the mass tables published in 2012 [17]. Up to now there was not observed any odd-odd cluster emitter.

TABLE I. Qvalues in MeV and decimal logarithm of the half-lives in seconds for the most probable CR and αD of cluster emitters experimentally observed.

Parent	Emitted	Q_c	$\log_{10} T_c^{exp}(s)$	$\log_{10} T_c^{ASAF}(s)$	Q_α	$\log_{10} T_\alpha^{exp}(s)$
^{221}Fr	^{14}C	31.291	14.52	14.27	6.458	2.55
^{221}Ra	^{14}C	32.395	13.39	13.74	6.881	1.90
^{222}Ra	^{14}C	33.049	11.01	11.15	6.679	1.58
^{223}Ra	^{14}C	31.828	15.19	14.72	5.979	5.99
^{224}Ra	^{14}C	30.534	15.86	15.93	5.789	5.50
^{226}Ra	^{14}C	28.196	21.19	20.98	4.870	10.70
^{223}Ac	^{14}C	33.064	12.96	12.68	6.783	2.48
^{225}Ac	^{14}C	30.476	17.28	17.69	5.935	6.23
^{228}Th	^{20}O	44.724	20.72	21.72	5.520	7.78
^{231}Pa	^{23}F	51.860	26.02	25.52	5.149	11.47
^{230}U	^{22}Ne	61.386	19.57	20.12	5.992	6.26
^{230}Th	^{24}Ne	57.760	24.61	24.86	4.770	12.38
^{231}Pa	^{24}Ne	60.409	23.23	23.01	5.149	11.47
^{232}U	^{24}Ne	62.309	20.42	20.37	5.413	9.34
^{233}U	^{24}Ne	60.485	24.84	24.97	4.909	12.78
^{234}U	^{24}Ne	58.824	25.92	25.72	4.857	13.04
^{235}U	^{24}Ne	57.362	27.42	29.97	4.678	16.57
^{233}U	^{25}Ne	60.727	24.84	25.48	4.909	12.78
^{235}U	^{25}Ne	57.706	27.42	30.38	4.678	16.57
^{234}U	^{26}Ne	59.415	25.92	26.59	4.857	13.04
^{234}U	^{28}Mg	74.109	25.14	25.34	4.857	13.04
^{236}Pu	^{28}Mg	79.668	21.52	20.55	5.867	7.95
^{238}Pu	^{28}Mg	75.909	25.70	25.60	5.593	9.44
^{236}U	^{30}Mg	72.274	27.58	29.54	4.573	14.99
^{238}Pu	^{30}Mg	76.795	25.70	25.86	5.593	9.44
^{238}Pu	^{32}Si	91.186	25.27	25.33	5.593	9.44
^{242}Cm	^{34}Si	96.509	23.15	22.77	6.216	7.15

It is clear that $T_c >> T_\alpha$, hence cluster radioactivity of nuclei with atomic numbers $Z = 87 - 96$ is a rare phenomenon in a huge background of α particles. The measurements are in good agreement with predictions within analytical superasymmetric fission (ASAF) model [28, 29]. Surprisingly, for some superheavy nuclei we found [16, 30] comparable half-lives or even shorter $T_c < T_\alpha$.

We expect that the same Q-values and half-lives will be observed in the future for anti-cluster decay and anti-alpha decay of antimatter nuclei. Perhaps the easiest way to observe the decay modes of antimatter nuclei would be to produce the lightest $\bar{\alpha}$ emiter, $^8\bar{B}e$, which will be split in two $^4\bar{H}e$ or two $\bar{\alpha}$ nuclei with a half-life of about $81.9 \cdot 10^{-18}$ s= 81.9 as — the same with that of $^8Be \to \alpha + \alpha$ [31].

ACKNOWLEDGMENTS

This work was supported within the IDEI Programme under Contracts No. 43/05.10.2011 and No. 42/05.10.2011 with UEFISCDI, and NUCLEU Programme, Bucharest.

[1] P. Dirac, Proc. Roy. Soc. Lond. **A 117**, 610 (1928).

[2] C. Anderson, Phys. Rev. **43**, 491 (1933).

[3] O. Chamberlain, E. Segrè, C. Wiegand, and T. Ypsilantis, Phys. Rev. **100**, 947 (1955).

[4] B. Cork, G. Lambertson, O. Piccioni, and W. Wenzel, Phys. Rev. **104**, 1193 (1956).

[5] A. Andronic, P. Braun-Munzinger, J. Stachel, and H. Stöcker, Phys. Lett. B **697**, 203 (2011).

[6] F. Close, *Antimatter* (Oxford University Press, New York, 2009).

[7] *Fundamental Physics in Particle Traps (Springer Tracts in Modern Physics 256)*, Eds. W. Quint, M. Vogel (Springer, Berlin, 2014).

[8] G. Baur *et al.*, Phys. Lett. B **368**, 251 (1996).

[9] G. Gabrielse *et al.*, Phys. Rev. Lett. **89**, 213401 (2002).

[10] G. Andresen *et al.*, Nature **468**, 673 (2010).

[11] ALPHA Collaboration, Nature Physics **7**, 558564 (2011).

[12] STAR Collaboration, Nature **473**, 353 (2011).

[13] W. Greiner, J. Phys.: Conf. Ser. **403**, 012046 (2012).

[14] Encyclopaedia Britannica Online http://www.britannica.com/EBchecked/topic/465998/.

[15] D. N. Poenaru, W. Greiner, in *Clusters in Nuclei Vol. 1. Lecture Notes in Physics 818*, Ed. C. Beck (Springer, Berlin, 2010), Chap. 1, pp. 1–56.

[16] D. N. Poenaru, R. A. Gherghescu, and W. Greiner, Phys. Rev. Lett. **107**, 062503 (2011).

[17] M. Wang *et al.*, Chinese Physics, C **36**, 16032014 (2012).

[18] D. N. Poenaru, M. Ivaşcu, D. Mazilu, Computer Physics Communications **19**, 205-214 (1980).

[19] G. Gamow, Z. Phys. **51**, 204 (1928).

[20] W. Greiner, J. A. Maruhn, *Nuclear Models* (Springer, Berlin, 1996).

[21] W. D. Myers, W. J. Swiatecki, Nucl. Phys. A **81**, 1 (1966).

[22] H. J. Krappe, J. R. Nix, A. J. Sierk, Phys. Rev. C **20**, 992 (1979).

[23] V. M. Strutinsky, Nucl. Phys. A **95**, 420 (1967).

[24] R. A. Gherghescu, Phys. Rev. C **67**, 014309 (2003).

[25] K. T. R. Davies, A. J. Sierk, J. Comput. Phys. **18**, 311 (1975).

[26] R. Bonetti, A. Guglielmetti, Rom. Rep. Phys. **59**, 301 (2007).

[27] A. Guglielmetti *et al.*, J. Phys.: Conf. Ser. **111**, 012050 (2008).

[28] D. N. Poenaru, W. Greiner *et al.*, Atomic Data Nucl. Data Tab. **34**, 423 (1986).

[29] D. N. Poenaru, D. Schnabel, W. Greiner, D. Mazilu, R. Gherghescu, Atomic Data Nucl. Data Tab. **48**, 231 (1991).

[30] D. N. Poenaru, R. A. Gherghescu, W. Greiner, Phys. Rev. C **85**, 034615 (2012).

[31] G. Audi *et al.*, Chinese Physics, C **36**, 11571286 (2012).

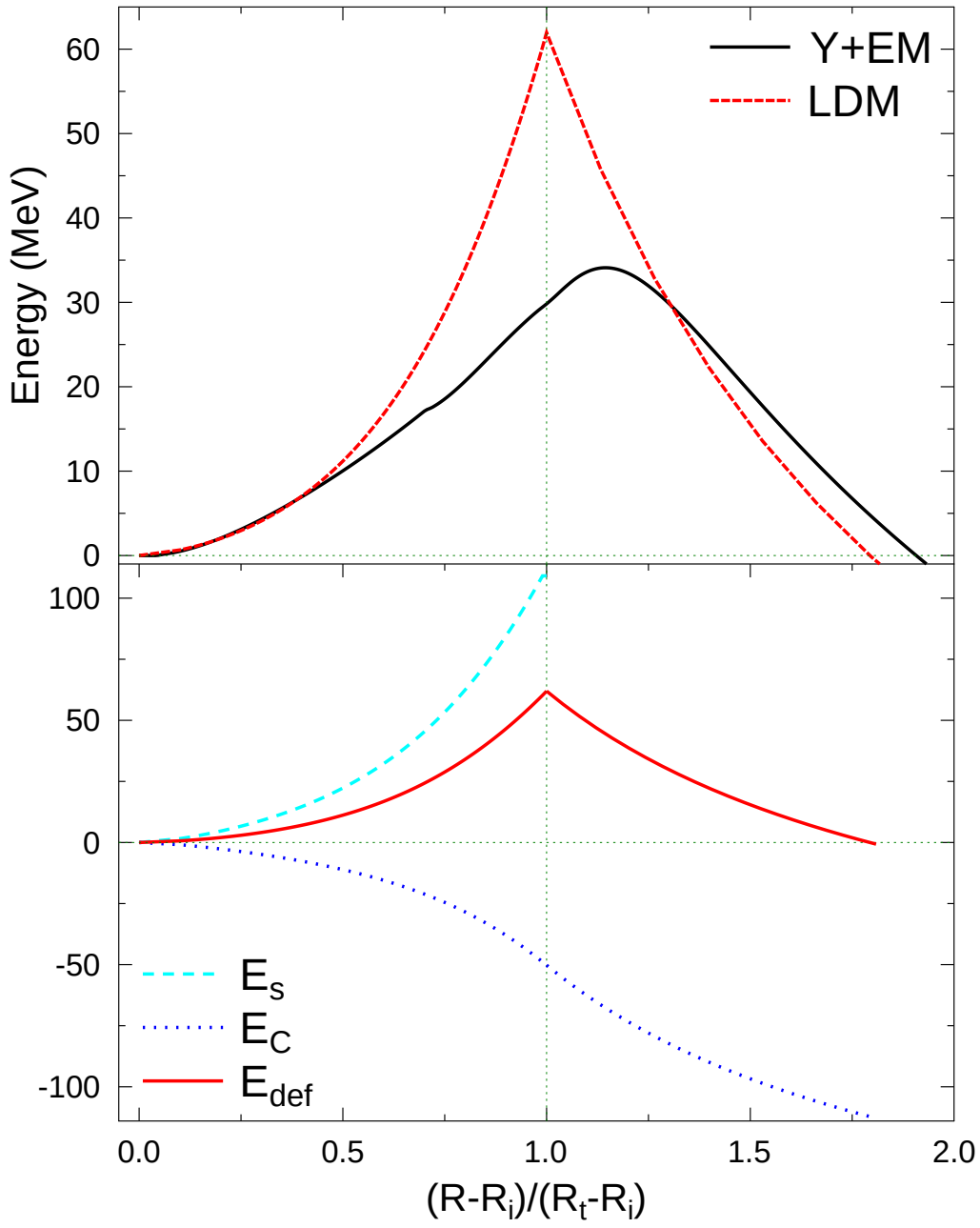

FIG. 1. (Color online) TOP: potential barrier for emission of $^{34}\bar{S}i$ from $^{242}\bar{C}m$ calculated within LDM (red) Y+EM (black). BOTTOM: two main terms of the LDM barrier: surface energy (dashed line cyan) and Coulomb energy (dotted line blue).

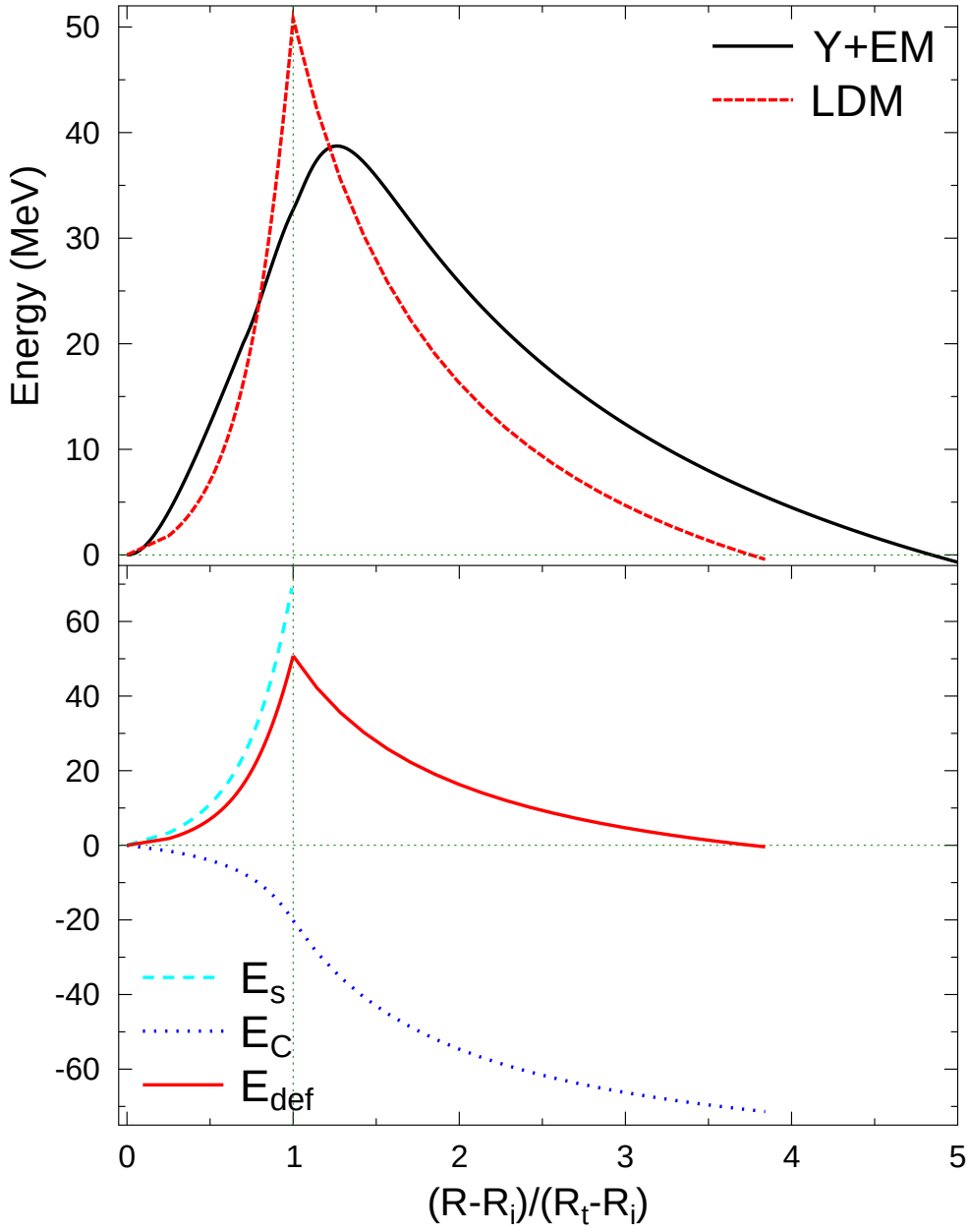

FIG. 2. (Color online) TOP: potential barrier for emission of $^{14}\bar{C}$ from $^{250}\bar{C}f$ calculated within LDM (red) Y+EM (black). BOTTOM: two main terms of the LDM barrier: surface energy (dashed line cyan) and Coulomb energy (dotted line blue).